AGU PUBLICATIONS

Geophysical Research Letters

RESEARCH LETTER
10.1002/2017GL072803

Key Points:
- Slow slip events reach the trench off the Nicoya Peninsula
- Slow slip events initiate in areas of high pore fluid pressure
- Elastic strain accumulates in shallow parts of subduction zone

Supporting Information:
- Supporting Information S1
- Movie S1

Correspondence to:
Y. Jiang,
yan.jiang@canada.ca

Citation:
Jiang, Y., Z. Liu, E. E. Davis, S. Y. Schwartz, T. H. Dixon, N. Voss, R. Malservisi, and M. Protti (2017), Strain release at the trench during shallow slow slip: The example of Nicoya Peninsula, Costa Rica, *Geophys. Res. Lett.*, *44*, 4846–4854, doi:10.1002/2017GL072803.

Received 25 JAN 2017
Accepted 11 MAY 2017
Accepted article online 26 MAY 2017
Published online 29 MAY 2017

Strain release at the trench during shallow slow slip: The example of Nicoya Peninsula, Costa Rica

Yan Jiang[1], Zhen Liu[2], Earl E. Davis[1], Susan Y. Schwartz[3], Timothy H. Dixon[4], Nick Voss[4], Rocco Malservisi[4], and Marino Protti[5]

[1]Geological Survey of Canada, Natural Resources Canada, Sidney, British Columbia, Canada, [2]Jet Propulsion Laboratory, California Institute of Technology, Pasadena, California, USA, [3]Department of Earth and Planetary Sciences, University of California, Santa Cruz, California, USA, [4]Department of Geology, University of South Florida, Tampa, Florida, USA, [5]Observatorio Vulcanológico y Sismológico de Costa Rica, Universidad Nacional, Heredia, Costa Rica

Abstract The near-trench behavior of subduction megathrust faults is critical for understanding earthquake hazard and tsunami generation. The shallow subduction interface is typically located in unconsolidated sediments that are considered too weak to accumulate elastic strain. However, the spectrum of shallow fault slip behavior is still elusive, due in large part to the lack of near-field observations. Here we combine measurements from seafloor pressure sensors near the trench and an onshore GPS network in a time-dependent inversion to image the initiation and migration of a well-documented slow slip event (SSE) in 2007 at the Nicoya Peninsula, Costa Rica. Our results show that the shallow SSE initiated on the shallow subduction interface at a depth of ~15 km, where pore fluid pressure is inferred to be high, and propagated all the way to the trench. The migrating event may have triggered a second subevent that occurred 1 month later. Our results document the release of elastic strain at the shallow part of the subduction megathrust and suggest prior accumulation of elastic strain. In conjunction with near-trench shallow slow slip recently reported for the Hikurangi subduction zone and trench breaching ruptures revealed in some large earthquakes, our results suggest that near-trench strain accumulation and release at the shallower portions of the subduction interface is more common than previously thought.

1. Introduction

Over the past decade, geodetically detected slow slip events (SSEs) and accompanying nonvolcanic tremor have been observed in many subduction zones, expanding the spectrum of known fault behaviors and providing insight into fault mechanics [e.g., *Dragert et al.*, 2001; *Rogers and Dragert*, 2003; *Schwartz and Rokosky*, 2007]. Although they do not release strain at the same rate as normal earthquakes, fault slip during SSEs is typically associated with shear failure on the plate interface [*Rubinstein et al.*, 2007]. These slips presumably follow a rate-and-state constitutive law [*Liu and Rice*, 2005]. Most observed SSEs are located downdip of seismogenic zones [*Schwartz and Rokosky*, 2007; *Schmidt and Gao*, 2010]. The shallow portion of the subduction interface updip of seismogenic zones is usually considered to be velocity strengthening, where frictional resistance increases with slip velocity, limiting fast slip propagation [*Scholz*, 1998]. In many places, the frontal prism has been thought to be too weak to accumulate elastic strain and to deform continuously throughout the seismic cycle [*Byrne et al.*, 1988]. However, this assumption is challenged by rare observations of interseismic strain accumulation near the trench [*Gagnon et al.*, 2005; *Davis et al.*, 2011] and occasional rapid rupture during seismic events [*Kanamori and Kikuchi*, 1993; *Fujiwara et al.*, 2011; *Newman et al.*, 2011]. Furthermore, in different subduction zones, shallow SSEs have been inferred from geodetic observations [*Vallee et al.*, 2013; *Dixon et al.*, 2014; *Wallace et al.*, 2016]. It is also important to note that the lack of observed shallow SSEs elsewhere may reflect the sampling bias resulting from the limited offshore resolution of onshore GPS networks. Another uncertainty in budgeting the spatial distribution of strain accumulation at a subduction interface, even in an area with inferred shallow SSEs, is whether such slip extends all the way to the trench. For this, direct seafloor observations near the deformation front are necessary. Since tsunami amplitudes are particularly sensitive to slip near the trench, understanding fault behavior and strain accumulation at the shallow portion of the plate interface is critical for understanding the tsunami process and for improved hazard mitigation [*Okal*, 1988].

The 2012 M_w 7.6 Nicoya earthquake is among a group of subduction zone events that lack shallow seismogenic rupture and a significant tsunami [*Protti et al.*, 2014] (Figure 1). Inversion of onshore GPS data suggests

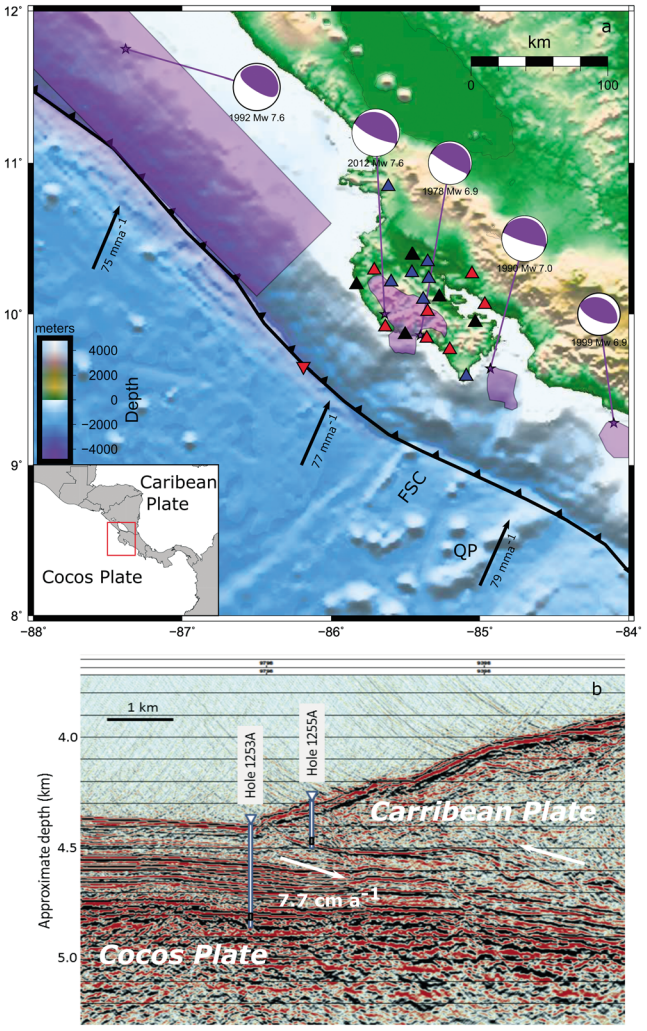

Figure 1. (a) Seismotectonic setting of the Nicoya Peninsula and adjacent area. Shaded areas are coseismic rupture areas of the 1990 Gulf of Nicoya earthquake [*Protti et al.*, 1995], 1992 Nicaragua earthquake [*Ihmlé*, 1996], 1999 Quepos earthquake [*Bilek et al.*, 2003], and 2012 Nicoya earthquake [*Yue et al.*, 2013]. Red triangles are locations of continuous GPS sites used in the inversion. Inverted red triangle is the location of the IODP Hole 1255A borehole observatory. Blue and black triangles are operating seismic stations and collocated GPS and seismic stations, respectively, that were operating at the time of the 2007 SSE. Fisher Seamount Chain (FSC) and Quepos Plateau (QP) are shown in the bathymetry map. (b) Cross-strike seismic reflection profile at the pressure monitoring sites (inverted triangle in Figure 1a). Formation pressure screen locations are shown with black rectangles filled with gray. Seafloor pressure sensors are shown with blue inverted triangle filled with gray. Modified from *Davis et al.* [2015] with permission from Elsevier.

that coseismic and transient slip regions are mutually exclusive; i.e., the coseismic rupture area is surrounded by slow slip and afterslip patches, both updip and downdip [*Dixon et al.*, 2014; *Malservisi et al.*, 2015]. This likely reflects different fault frictional properties on the plate interface. Shallow SSEs have been reported beneath the Nicoya Peninsula and have been suggested as one of the reasons for the lack of tsunami in the region [*Dixon et al.*, 2014]. Slip to the trench has been suggested in Nicoya [*Davis et al.*, 2015], but the connection between shallow SSEs and slip penetrating fully to the trench remains unclear. In Hikurangi, *Wallace et al.* [2016] suggest that slow slip propagates to within 2 km landward of the trench by using a seafloor pressure network. Their near-trench resolution is low owing to the lack of observing sites at the trench. Offshore the Nicoya Peninsula, two seafloor pressure recorders are installed in the Middle America trench, one on the incoming Cocos plate and the other 800 m landward on the prism toe, providing direct observation of seafloor displacement during SSEs (Figure 1). Here we report the first examination of transient slip behavior at the Nicoya Peninsula, Costa Rica, that combines onshore GPS and offshore seafloor pressure measurements of an SSE in 2007. We show that the observations are consistent with slow but continuous propagation of slip from a deeper source to the trench.

2. Data and Processing Methods

Onshore continuous GPS (cGPS) was first installed at the Nicoya Peninsula in 2002 and has been expanding since then (Figure 1). The first slow slip event was observed by this network in 2003 [*Protti et al.*, 2004], with similar events occurring about every 2 years [*Jiang et al.*, 2012]. By the time of the 2007 SSE, a total of 12 operating cGPS sites provided three-component position time series. We used raw RINEX files downloaded from UNAVCO data archive (www.unavco.org/data/data.html) and GIPSY v6.3 from Jet Propulsion Lab (JPL; https://gipsy-oasis.jpl.nasa.gov/) to compute daily coordinates for each station. We adopted precise point positioning strategy in our data analysis [*Zumberge et al.*, 1997]. Wide Lane Phase Bias files provided by JPL were used to resolve single receiver ambiguity [*Bertiger et al.*, 2010]. The precise

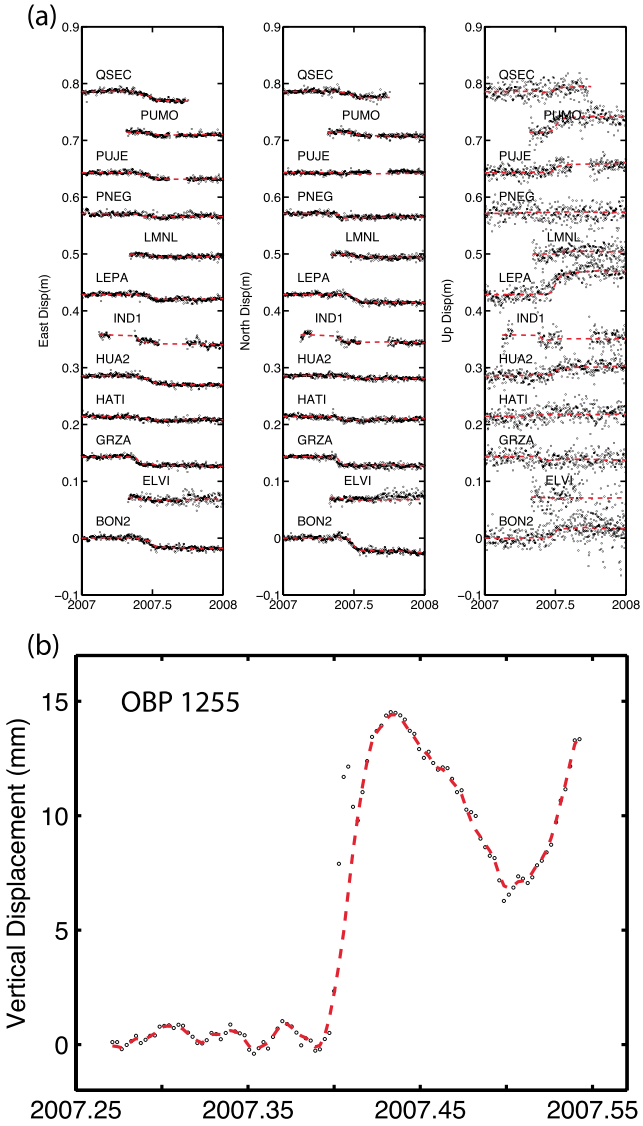

Figure 2. GPS and OBP time series and model fit. Red dashed lines are time-dependent model predictions at all locations. Black circles are (a) positions time series of GPS stations and (b) vertical movements of ocean bottom pressure site 1255. We used 12 GPS sites and the differential vertical displacement at OBP site 1255 to invert slow slip in the vicinity of the Nicoya Peninsula. Horizontal displacements at site 1255 are arbitrarily set to 0, with large uncertainties (2 m) assigned to the data in order to deweight the horizontal components. The GPS data and model fit have been scaled by a factor of 2 to better show the SSE signals. OBP vertical data and model fit are not scaled.

orbit and satellite clock files from JPL using a globally distributed network were used in the analysis. We excluded daily observations with less than 4 h of observations. Numerical predictions from the Vienna Mapping Functions were used to correct propagation time delay induced by water vapor in the troposphere [*Boehm et al.*, 2006]. Daily coordinates were first evaluated in a loosely constrained reference frame and then aligned to the IGb08 reference frame [*Rebischung et al.*, 2012] through a seven-parameter transformation. We applied a least-square algorithm that simultaneously fit the long-term linear trend, seasonal signal, and slow slip event to the daily raw time series [details see *Jiang et al.*, 2012]. The post-fit weighted root mean squares for the raw time series are ~3 mm, ~3 mm, and ~8 mm for the north, east, and vertical components, respectively. A regional common mode filter was used to remove common mode error from the same regional noise sources [*Wdowinski et al.*, 1997]. Regional filtering reduced the post-fit weighted root mean squares to ~2mm, ~2mm, and ~6mm for the three components. We calculated and removed the linear trend and seasonal (annual and semiannual) signal in the filtered time series and used the corrected time series in the slip modeling.

Two offshore Circulation Obviation Retrofit Kit instruments were installed in 2002, providing continuous monitoring of formation pressure and seafloor pressure just above the prism toe décollement and within the incoming oceanic crust [*Davis and Villinger*, 2006] (Figure 1). In Nicoya the presence of borehole measurements at two stations ~800 m apart and spanning the seafloor locus of the subduction thrust provides unique data to test if slow slip extends to the trench. Changes of formation fluid pressure result from episodic volumetric strain disturbance caused by slip close to the trench [*Davis et al.*, 2011, 2015]. Changes in seafloor pressure result from vertical seafloor displacement; specifically, displacement of the prism relative to the incoming plate can be determined from the difference in absolute seafloor pressure between the two sites [*Davis et al.*, 2015; *Bürgmann and Chadwell*, 2014]. This is included with GPS data in our geodetic inversion (Figure 2). By differencing the measurements from the two closely spaced pressure sensors, we remove common

oceanic noise sources. Seafloor pressure time series are first detrended to remove instrumental drifts of −0.04 and +0.5 kPa/yr, equivalent to 0.4 and 5 cm/yr change in water depth, at Holes 1253A and 1255A, respectively. Resultant averaged daily vertical differential displacement time series have uncertainties of less than 2 mm (Figures S1 and S2 in the supporting information), enabling detection of small seafloor uplift. The prism site (site 1255A) is ~700 m landward of the prism toe, and differential pressure shows uplift during the 2007 SSE, suggesting slip to the trench during this event.

In addition to the GPS and seafloor pressure instruments, 13 broadband and short period seismometers were operating in the same region at the time of the 2007 SSE (Figure 1). We used data from this seismic network and a modified version of the envelope cross-correlation method [*Wech and Creager*, 2008] to detect and locate tremor (Figure S3) and compare its spatiotemporal distribution to that of the 2007 slow slip (Movie S1). In order not to mistake the abundant microseismicity as tremor, we band-pass filtered east component data in two frequency ranges before creating and cross-correlating envelope functions, a tremor band between 2 to 5 Hz and an earthquake band between 8 to 20 Hz. Tremor detection occurred when cross-correlation coefficients exceeded a value of 0.6 on more than 10 station pairs filtered in the tremor band and did not exceed a value of 0.6 on more than five station pairs filtered in the earthquake band [for details see *Kim et al*., 2011].

3. Time-Dependent Model

We applied a modified network inversion filter [e.g., *Segall and Matthews*, 1997; *McGuire and Segall*, 2003; *Liu et al*., 2010, 2015] to model time-varying deformation signals and spatiotemporal evolution of transient fault slip on the megathrust interface beneath the Nicoya Peninsula. We used the combination of onshore GPS and offshore seafloor pressure sensors and focused on the 2007 SSE, a well-studied event [*Outerbridge et al*., 2010; *Dixon et al*., 2014]. We validate the earlier static inversion results and expand the geographic coverage and improve offshore resolution by including the seafloor pressure data at the prism toe. The modeling includes positivity and spatial smoothing constraints, incorporates observations and constraints into a state-space model of system and measurement process, and solves for slip distribution using an extended Kalman filter. We model the interplate thrust surface with a triangular mesh that takes into account complex three-dimensional fault geometry. We use the interplate fault geometry from Slab1.0 [*Hayes et al*., 2012] and construct the triangular grid from discrete isodepth contour points. We calculate the elastostatic Green's function using triangular dislocation elements [*Jeyakumaran et al*., 1992] and perform spatial smoothing on a triangular surface based on the Fujiwara operator [*Desbrun et al*., 1999]. We assume that transient deformation due to slow slip results mainly from reverse slip on the subduction thrust interface. Including a strike-slip component in the modeling does not improve the data fit. We impose a nonnegative constraint in the slip inversion. The GPS benchmark motion is modeled as a random walk [*Agnew*, 1992; *Langbein and Johnson*, 1997] with scale parameter τ = 0.5 mm/$\sqrt{\text{yr}}$. The average mesh size in our triangular mesh is ~23 km. Using a smaller mesh size or a larger benchmark wobble term (e.g., 1 mm/$\sqrt{\text{yr}}$) does not change the results. We select the optimal hyperparameters for temporal and spatial smoothing through a grid search and the inspection of trade-off between the data fit and the roughness of the resultant slip distribution. Cleaned and filtered three-component position time series from ~12 continuous GPS sites from the Costa Rica GPS network, along with the vertical displacement derived from the seafloor differential pressure data, were used to invert for slip history of the 2007 slow slip event (Figure 2).

4. Inversion Results

Adding the seafloor pressure data has greatly improved our network resolution offshore (Figure S4). By adding one OBP site, our resolution test shows dramatic increase of network sensitivity to the near trench slip (Figure S4c). For the deeper megathrust, the new slip distribution from our time-dependent inversion stays unchanged compared to earlier results [*Dixon et al*., 2014], but we are now able to estimate the offshore slip distribution (Figure 3) and slip migration during the course of the 2007 SSE (Figure 4). We find one slip patch centered 25–30 km landward from the trench, with a maximum slip of ~10 cm. The slip decreases seaward from the peak amplitude and reaches to the trench with ~5 cm of slip. The area of slip includes a number of structures related to fluid seepage [*Sahling et al*., 2008], experienced fluid flow anomalies during a transient event in 2000 [*Brown et al*., 2005], and is believed to be rich in fluid released from subducted marine sediments [*Saffer and Tobin*, 2011]. All suggest an underlying fluid source that is probably overpressured.

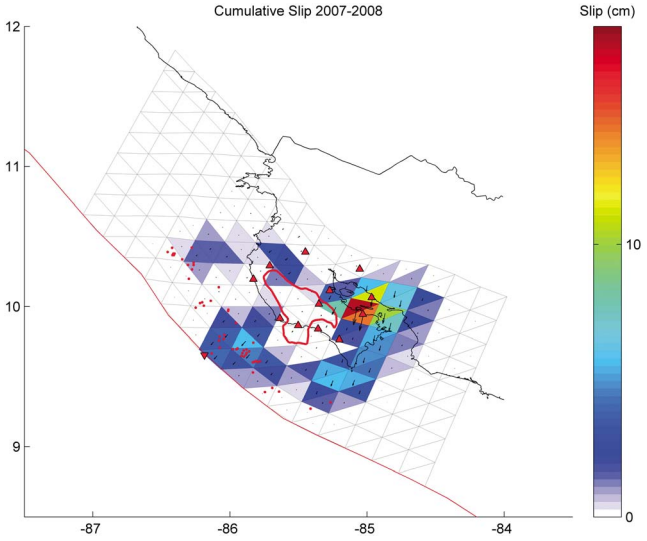

Figure 3. Accumulated slip of the 2007 SSE. Red triangles are locations of continuous GPS sites used in the inversion. Inverted red triangle is the location of the IODP Hole 1255A borehole observatory. Model area is divided into discrete triangle elements, with an average mesh size of 23 km. Color represents the amplitude of accumulated slip within each triangle element. Arrows represent slip directions on the plate interface. Solid red line outlines the coseismic rupture area of the 2012 Nicoya earthquake [*Yue et al*., 2013]. Red dots show the locations of identified seafloor fluid seepage [*Sahling et al*., 2008].

Our time-dependent inversion results provide information on slip propagation (Movie S1). We find that slow slip initiates at the shallow and updip portion of the coseismic rupture area in the 2012 Nicoya earthquake (Figure 4). The location of initiation matches the patch of maximum slip in the shallow portion and is collocated with areas of high pore fluid pressure [*Saffer and Tobin*, 2011]. The 2007 SSE initiated on day of year (DOY) 136 (16 May 2007), coincident with the onset of shallow tremor, then propagated in both dip and strike directions. Downdip slip propagation is faster than updip and along-strike propagation. The slip front has a downdip propagation speed of ~4 km/day, reaching the updip limit of coseismic rupture of the 2012 Nicoya earthquake by around DOY 141. The slip front may have propagated continuously downdip, around the 2012 Nicoya asperity (Figure 4). Similar to results in the static inversion [*Dixon et al*., 2014], our time-dependent results show very little or no slow slip occurs inside the 1990 and 2012 earthquake asperities, presumably reflecting fundamental differences in frictional conditions and the state of stress. The onset of prism toe deformation is well defined by both formation pressure change near the décollement and the episode of seafloor uplift recorded by seafloor pressure sensors (Figure S5). Slip propagates updip at a speed of about 2 km/day and reaches the trench on DOY 146. In the meantime, slip migrates along-strike to the southeast of the Nicoya Peninsula at a similar speed. A second subevent occurs approximately 1 month after the onset of the shallow event, around DOY 168. This subevent expands into both shallow and deep portions of the subduction interface, producing a maximum accumulated slip of ~20 cm. No transients are seen at the prism toe sites at the time of this event, however, suggesting that this subevent did not propagate to the trench near site 1255A. The start time of the second subevent correlates well with the time when the first event propagated to the updip portion of the second subevent (Figure S6), suggesting possible triggering of the deep slow slip by the shallow event.

In the area of the shallow SSEs in Costa Rica, pore pressure is estimated to be close to lithostatic [*Saffer and Tobin*, 2011]. Thus, this region may be in a critical state subject to triggering of transient events by small stress perturbations. Static and dynamic triggering of SSEs by small stress changes (a few kPa) have been found worldwide [*Peng and Gomberg*, 2010]. Past studies have shown a 10 kPa increase of coulomb failure stress associated with a similar SSE in the Nicoya Peninsula [*Dixon et al.,* 2014]. To test whether the initiation of the second subevent may be partly promoted by shallow transient slip, we calculated the coulomb stress change on the plate interface resulting from the first shallow subevent. We used a nominal friction coefficient of 0.6. The calculated coulomb stress increase at the deep slip area ranges from 5 to 20 kPa (Figure S7), which is comparable to past triggering stress threshold found elsewhere [*Wallace et al*., 2012; *Davis et al.,* 2013], suggesting that triggering of the second slip subevent cannot be excluded.

5. Discussion and Conclusions

Our results, along with evidence from observations at the Hikurangi margin, New Zealand [*Wallace et al*., 2016], and Nankai trough, Japan [*Davis et al*., 2006, 2013], suggest that cases of rupture to the trench during

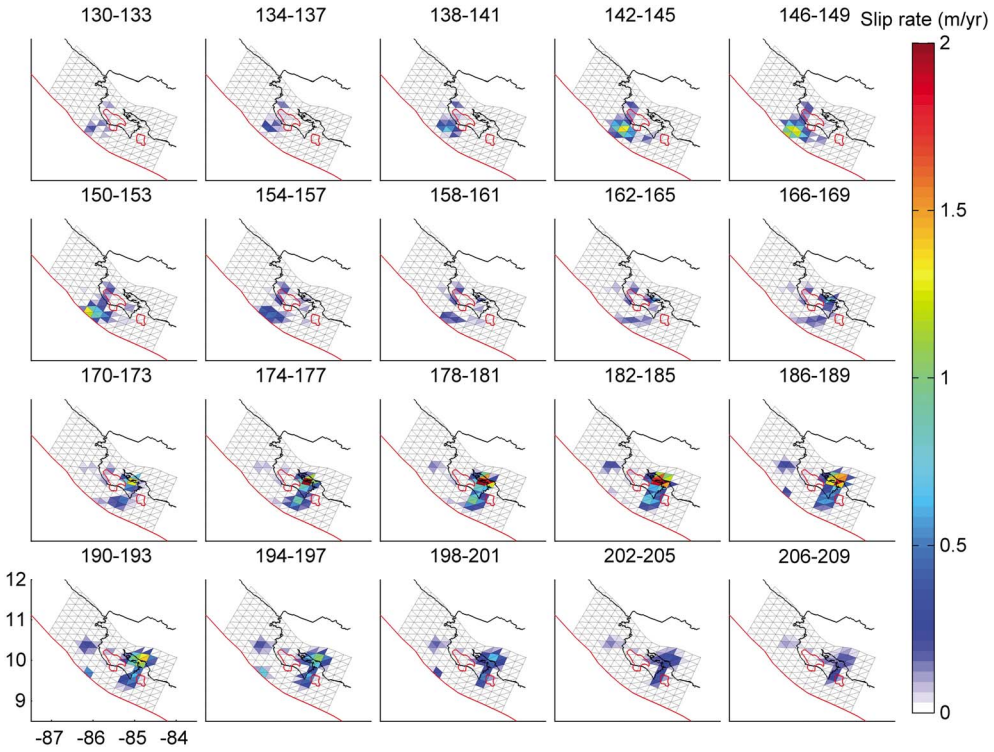

Figure 4. Time-dependent slip history of the 2007 SSE. Color represents average slip rate within each element. Title of each subplot is the day-of-year (DOY) range of the subplot. Red lines are the coseismic rupture area of the 1990 Gulf of Nicoya earthquake [*Protti et al*., 1995] and 2012 Nicoya earthquake [*Yue et al*., 2013].

aseismic events are more common than previously thought. Unlike Hikurangi and Nankai, the Nicoya GPS and seafloor pressure network is able to resolve ~5 cm of slip to the trench during the 2007 event with confidence. The pressure monitoring site is within 700 meters of the deformation front and shows delayed seafloor uplift following several other slow slip events detected by onshore GPS and accompanied by offshore nonvolcanic tremor [*Davis et al*., 2015; *Walter et al*., 2013], implying that slip propagating to the trench from a deeper source is common at the Nicoya Peninsula. Frequent slip at the trench highlights the importance of understanding shallow source areas in accumulating strain, hosting seismic and aseismic slip, and tsunamigenesis. Our result suggests that portions of the shallowest part of the subduction zone are at least strong enough to accumulate a slip deficit between its frequent SSEs. However, the fact that no SSE initiates at the trench [*Davis et al*., 2015] may suggest that the trench portion of the interface acts only in response to slip at deeper levels. To address this and to obtain a more comprehensive understanding of shallow fault behavior for better tsunami hazard assessment and mitigation, further continuous monitoring of strain accumulation and release in the shallowest parts of subduction zones will be required.

The very shallow portions of the subduction interface are typically characterized by very low temperature and pressure. Transitional frictional conditions are often attributed to the genesis of slow slip on the subduction interface [e.g., *Liu et al*., 2005]. Both shallow slow slip and tsunami earthquakes are thought to occur under transitional frictional conditions [*Bilek and Lay*, 2002; *Saffer and Wallace*, 2015] under which seismic slip can propagate. Thus, the possibility that transitional friction conditions might extend all the way to the trench in the offshore region of the Nicoya Peninsula cannot be excluded. Heterogeneities in frictional conditions at the very shallow portions of the plate interface are likely, and we expect that locally high pore fluid pressure may also play a role in generating the shallow slow slip events in Costa Rica. The shallow plate interface is generally considered to be a high pore fluid pressure environment due to compaction and dehydration of subducted oceanic sediments [*Saffer and Tobin*, 2011]. In Nicoya similar fluid-rich conditions have also been suggested for the deep SSE zone based on seismic [*Audet and Schwartz*, 2013] and magnetotelluric

[*Worzewski et al*., 2011] studies. These observations suggest that both deep and shallow SSEs may be driven by similar mechanisms. The thin upper plate at shallow depth and elevated pore fluid pressure at both the shallow and deep subduction interface serve to reduce the effective normal stress, increasing the width of the conditionally stable zone and facilitating the occurrence of slow slip [*Kodaira et al*., 2004].

Just how spatially or temporally representative the behavior of the seaward part of the subduction thrust described here might be difficult to say, and much needs to be learned before generalizing the observations. Immediately to the north along the Mid-American Trench, a tsunami earthquake struck Nicaragua in 1992, rupturing all the way to the trench [*Kanamori and Kikuchi*, 1993] (Figure 1). An extreme example of tsunamigenic slip to the trench occurred during the Tohoku-oki subduction earthquake [*Fujiwara et al*., 2011]. The Nicoya Peninsula has not experienced a severe tsunami in recorded history. However, from 2006 to 2011, five episodes of seafloor uplift similar to the 2007 event have been documented at the same sites offshore Nicoya [*Davis et al*., 2015]. These observations indicate that elastic strain can be released slowly at the prism toe, with no seismogenesis or tsunamigenesis in the shallow subduction interface of the Nicoya Peninsula. Evidence of seamount subduction beneath the Nicoya Peninsula has been found [*Kyriakopoulos et al*., 2015], and seamounts certainly play a role in the subduction system. But it is not clear whether seamounts will promote or inhibit large thrust earthquakes in subduction zones [*Scholz and Small*, 1997; *Wang and Bilek*, 2011]. In this paper, we focus on the shallow portion of the subduction zone where the subducted oceanic plate is relatively smooth; thus, our interpretation is not biased by the subducted seamount. If we assume a similar 5–10 cm slip for each of the shallow SSEs between 2006 and 2011 and recurrent nature of these shallow SSEs, it would appear that shallow SSEs offshore of the Nicoya Peninsula may be sufficient to accommodate plate motion; i.e., strain may not be accumulating over the long term. Of course, it is possible that tsunamigenic earthquakes occur here, but with much longer recurrence intervals. *Goldfinger et al.* [2013] note that subduction zone earthquakes can cluster in time, with the largest event tending to occur near the end of the cluster, consistent with an accumulating slip deficit over several seismic cycles. We cannot preclude small amounts of strain, below the resolution of our data, accumulating over multiple slow slip cycles. Only continuing observations will resolve this question.

Acknowledgments
We thank UNAVCO for archiving and providing access to raw GPS data, Jet Propulsion Lab (JPL) for providing the GIPSY software, Honn Kao for providing internal review of the paper, and Kelin Wang for discussions. Comments from Brendan Crowell and from Editor Jeroen Ritsema helped to improve the manuscript. Research at the Geological Survey of Canada was supported by the Public Safety and Geoscience Program, research at the Jet Propulsion Laboratory, California Institute of Technology was supported by NASA's Earth Surface and Interior focus area. T.H.D. and N.V. were supported in part by NSF/EAR 1345100. This is Geological Survey of Canada contribution 20160443.

References

Agnew, D. (1992), The time-domain behavior of power-law noises, *Geophys. Res. Lett.*, *19*(4), 333–336, doi:10.1029/91GL02832.
Audet, P., and S. Y. Schwartz (2013), Hydrologic control of forearc strength and seismicity in the Costa Rican subduction zone, *Nat. Geosci.*, *6*(10), 852–855.
Bertiger, W., S. D. Desai, B. Haines, N. Harvey, A. W. Moore, S. Owen, and J. P. Weiss (2010), Single receiver phase ambiguity resolution with GPS data, *J. Geod.*, *84*(5), 327–337.
Bilek, S. L., and T. Lay (2002), Tsunami earthquakes possibly widespread manifestations of frictional conditional stability, *Geophys. Res. Lett.*, *29*(14), 1673, doi:10.1029/2002GL015215.
Bilek, S. L., S. Y. Schwartz, and H. R. DeShon (2003), Control of seafloor roughness on earthquake rupture behavior, *Geology*, *31*(5), 455–458.
Boehm, J., B. Werl, and H. Schuh (2006), Troposphere mapping functions for GPS and very long baseline interferometry from European Centre for Medium-Range Weather Forecasts operational analysis data, *J. Geophys. Res.*, *111*, B02406, doi:10.1029/2005JB003629.
Brown, K. M., M. D. Tryon, H. R. DeShon, L. M. Dorman, and S. Y. Schwartz (2005), Correlated transient fluid pulsing and seismic tremor in the Costa Rica subduction zone, *Earth Planet. Sci. Lett.*, *238*(1), 189–203.
Bürgmann, R., and D. Chadwell (2014), Seafloor geodesy, *Annu. Rev. Earth Planet. Sci.*, *42*, 509–534.
Byrne, D. E., D. M. Davis, and L. R. Sykes (1988), Loci and maximum size of thrust earthquakes and the mechanics of the shallow region of subduction zones, *Tectonics*, *7*(4), 833–857.
Davis, E., M. Kinoshita, K. Becker, K. Wang, Y. Asano, and Y. Ito (2013), Episodic deformation and inferred slow slip at the Nankai subduction zone during the first decade of CORK borehole pressure and VLFE monitoring, *Earth Planet. Sci. Lett.*, *368*, 110–118.
Davis, E. E., and H. W. Villinger (2006), Transient formation fluid pressures and temperatures in the Costa Rica forearc prism and subducting oceanic basement: CORK monitoring at ODP Sites 1253 and 1255, *Earth Planet. Sci. Lett.*, *245*(1), 232–244.
Davis, E. E., K. Becker, K. Wang, K. Obara, Y. Ito, and M. Kinoshita (2006), A discrete episode of seismic and aseismic deformation of the Nankai trough subduction accretionary prism and incoming Philippine Sea plate, *Earth Planet. Sci. Lett.*, *242*, 73–84.
Davis, E. E., M. Heesemann, and K. Wang (2011), Evidence for episodic aseismic slip across the subduction seismogenic zone off Costa Rica: CORK borehole pressure observations at the subduction prism toe, *Earth Planet. Sci. Lett.*, *306*, 299–305.
Davis, E. E., H. Villinger, and T. Sun (2015), Slow and delayed deformation and uplift of the outermost subduction prism following ETS and seismogenic slip events beneath Nicoya Peninsula, Costa Rica, *Earth Planet. Sci. Lett.*, *410*, 117–127.
Desbrun, M., M. Meyer, P. Schröder, and A. H. Barr (1999), Implicit fairing of irregular meshes using diffusion and curvature flow, in *Proceedings of the 26th Annual Conference on Computer Graphics and Interactive Techniques, International Conference on Computer Graphics and Interactive Techniques*, pp. 317–324, ACM Press/Addison-Wesley Publishing Co., New York, doi:10.1145/311535.311576.
Dixon, T. H., Y. Jiang, R. Malservisi, R. McCaffrey, N. Voss, M. Protti, and V. Gonzalez (2014), Earthquake and tsunami forecasts: Relation of slow slip events to subsequent earthquake rupture, *Proc. Natl. Acad. Sci. U.S.A.*, *111*(48), 17,039–17,044.
Dragert, H., K. Wang, and T. S. James (2001), A silent slip event on the deeper Cascadia subduction interface, *Science*, *292*(5521), 1525–1528.

Fujiwara, T., S. Kodaira, Y. Kaiho, N. Takahashi, and Y. Kaneda (2011), The 2011 Tohoku-Oki earthquake: Displacement reaching the trench axis, *Science*, *334*(6060), 1240–1240.
Gagnon, K., C. D. Chadwell, and E. Norabuena (2005), Measuring the onset of locking in the Peru–Chile trench with GPS and acoustic measurements, *Nature*, *434*(7030), 205–208.
Goldfinger, C., Y. Ikeda, R. S. Yeats, and J. Ren (2013), Superquakes and supercycles, *Seismol. Res. Lett.*, *84*, 24–32.
Hayes, G. P., D. J. Wald, and R. L. Johnson (2012), Slab1.0: A three-dimensional model of global subduction zone geometries, *J. Geophys. Res.*, *117*, B01302, doi:10.1029/2011JB008524.
Ihmlé, P. F. (1996), Monte Carlo slip inversion in the frequency domain: Application to the 1992 Nicaragua slow earthquake, *Geophys. Res. Lett.*, *23*(9), 913–916, doi:10.1029/96GL00872.
Jeyakumaran, M., J. W. Rudnicki, and L. M. Keer (1992), Modeling slip zones with triangular dislocation elements, *Bull. Seismol. Soc. Am.*, *83*(5), 2153–2169.
Jiang, Y., S. Wdowinski, T. H. Dixon, M. Hackl, M. Protti, and V. Gonzalez (2012), Slow slip events in Costa Rica detected by continuous GPS observations, 2002–2011, *Geochem. Geophys. Geosyst.*, *13*, Q04006, doi:10.1029/2012GC004058.
Kanamori, H., and M. Kikuchi (1993), The 1992 Nicaragua earthquake: A slow tsunami earthquake associated with subducted sediments, *Nature*, *361*(6414), 714–716.
Kim, M. J., S. Y. Schwartz, and S. Bannister (2011), Non-volcanic tremor associated with the March 2010 Gisborne slow slip event at the Hikurangi subduction margin, New Zealand, *Geophys. Res. Lett.*, *38*, L14301, doi:10.1029/2011GL048400.
Kodaira, S., T. Iidaka, A. Kato, J. O. Park, T. Iwasaki, and Y. Kaneda (2004), High pore fluid pressure may cause silent slip in the Nankai Trough, *Science*, *304*(5675), 1295–1298.
Kyriakopoulos, C., A. V. Newman, A. M. Thomas, M. Moore-Driskell, and G. T. Farmer (2015), A new seismically constrained subduction interface model for Central America, *J. Geophys. Res. Solid Earth*, *120*, 5535–5548, doi:10.1002/2014JB011859.
Langbein, J., and H. Johnson (1997), Correlated errors in geodetic time series: Implications for time-dependent deformation, *J. Geophys. Res.*, *102*, 591–603, doi:10.1029/96JB02945.
Liu, Y., and J. R. Rice (2005), Aseismic slip transients emerge spontaneously in three-dimensional rate and state modeling of subduction earthquake sequences, *J. Geophys. Res.*, *110*, B08307, doi:10.1029/2004JB003424.
Liu, Z., S. Owen, D. Dong, P. Lundgren, F. Webb, E. Hetland, and M. Simons (2010), Integration of transient strain events with models of plate coupling and areas of great earthquakes in southwest Japan, 181, 1292-1312, *Geophys. J. Int.*, doi:10.1111/j.1365-246X.2010.04599.x.
Liu, Z., A. W. Moore, and S. Owen (2015), Recurrent slow slip event reveals the interaction with seismic slow earthquakes and disruption from large earthquake, *Geophys. J. Int.*, *202*(3), 1555–1565, doi:10.1093/gji/ggv238.
Malservisi, R., et al. (2015), Multiscale postseismic behavior on a megathrust: The 2012 Nicoya earthquake, Costa Rica, *Geochem. Geophys. Geosyst.*, *16*, 1848–1864, doi:10.1002/2015GC005794.
McGuire, J., and P. Segall (2003), Imaging of aseismic fault slip transients recorded by dense geodetic networks, *Geophys. J. Int.*, *155*, 778–788.
Newman, A. V., G. Hayes, Y. Wei, and J. Convers (2011), The 25 October 2010 Mentawai tsunami earthquake, from real-time discriminants, finite-fault rupture, and tsunami excitation, *Geophys. Res. Lett.*, *38*, L05302, doi:10.1029/2010GL046498.
Okal, E. A. (1988), Seismic parameters controlling far-field tsunami amplitudes: A review, *Nat. Hazards*, *1*(1), 67–96.
Outerbridge, K. C., T. H. Dixon, S. Y. Schwartz, J. I. Walter, M. Protti, V. Gonzalez, and W. Rabbel (2010), A tremor and slip event on the Cocos-Caribbean subduction zone as measured by a global positioning system (GPS) and seismic network on the Nicoya Peninsula, Costa Rica, *J. Geophys. Res.*, *115*, B10408, doi:10.1029/2009JB006845.
Peng, Z., and J. Gomberg (2010), An integrated perspective of the continuum between earthquakes and slow-slip phenomena, *Nat. Geosci.*, doi:10.1038/NGE0940.
Protti, M., et al. (1995), The March 25, 1990 (M_w = 7.0, M_L = 6.8), earthquake at the entrance of the Nicoya Gulf, Costa Rica: Its prior activity, foreshocks, aftershocks, and triggered seismicity, *J. Geophys. Res.*, *100*(B10), 20,345–20,358, doi:10.1029/94JB03099.
Protti, M., V. González, T. Kato, T. Iinuma, S. Miyazaki, K. Obana, Y. Kaneda, P. La Femina, T. Dixon, and S. Schwartrz (2004), A creep event on the shallow interface of the Nicoya Peninsula, Costa Rica seismogenic zone, AGU Fall Meeting Abstracts, vol. 1, p. 07.
Protti, M., V. González, A. V. Newman, T. H. Dixon, S. Y. Schwartz, J. S. Marshall, L. Feng, J. I. Walter, R. Malservisi, and S. E. Owen (2014), Nicoya earthquake rupture anticipated by geodetic measurement of the locked plate interface, *Nat. Geosci.*, *7*(2), 117–121.
Rebischung, P., J. Griffiths, J. Ray, R. Schmid, X. Collilieux, and B. Garayt (2012), IGS08: The IGS realization of ITRF2008, *GPS Solutions*, *16*(4), 483–494.
Rogers, G., and H. Dragert (2003), Episodic tremor and slip on the Cascadia subduction zone: The chatter of silent slip, *Science*, *300*(5627), 1942–1943.
Rubinstein, J. L., J. E. Vidale, J. Gomberg, P. Bodin, K. C. Creager, and S. D. Malone (2007), Non-volcanic tremor driven by large transient shear stresses, *Nature*, *448*(7153), 579–582.
Saffer, D. M., and H. J. Tobin (2011), Hydrogeology and mechanics of subduction zone forearcs: Fluid flow and pore pressure, *Annu. Rev. Earth Planet. Sci.*, *39*, 157–186.
Saffer, D. M., and L. M. Wallace (2015), The frictional, hydrologic, metamorphic and thermal habitat of shallow slow earthquakes, *Nat. Geosci.*, *8*(8), 594–600.
Sahling, H., D. G. Masson, C. R. Ranero, V. Hühnerbach, W. Weinrebe, I. Klaucke, D. Bürk, W. Brückmann, and E. Suess (2008), Fluid seepage at the continental margin offshore Costa Rica and southern Nicaragua, *Geochem. Geophys. Geosyst.*, *9*, Q05S05, doi:10.1029/2008GC001978.
Scholz, C. H. (1998), Earthquakes and friction laws, *Nature*, *391*(6662), 37–42.
Scholz, C. H., and C. Small (1997), The effect of seamount subduction on seismic coupling, *Geology*, *25*(6), 487–490.
Schmidt, D. A., and H. Gao (2010), Source parameters and time-dependent slip distributions of slow slip events on the Cascadia subduction zone from 1998 to 2008, *J. Geophys. Res.*, *115*, B00A18, doi:10.1029/2008JB006045.
Schwartz, S. Y., and J. M. Rokosky (2007), Slow slip events and seismic tremor at circum-Pacific subduction zones, *Rev. Geophys.*, *45*, RG3004, doi:10.1029/2006RG000208.
Segall, P., and M. Matthews (1997), Time dependent inversion of geodetic data, *J. Geophys. Res.*, *102*, 22,391–22,409.
Vallee, M., et al. (2013), Intense interface seismicity triggered by a shallow slow slip event in the Central Ecuador subduction zone, *J. Geophys. Res. Solid Earth*, *118*, 2965–2981, doi:10.1002/jgrb.50216.
Wallace, L. M., J. Beavan, S. Bannister, and C. Williams (2012), Simultaneous long-term and short-term slow slip events at the Hikurangi subduction margin, New Zealand: Implications for processes that control slow slip event occurrence, duration, and migration, *J. Geophys. Res.*, *117*, B11402, doi:10.1029/2012JB009489.
Wallace, L. M., S. C. Webb, Y. Ito, K. Mochizuki, R. Hino, S. Henrys, S. Y. Schwartz, and A. F. Sheehan (2016), Slow slip near the trench at the Hikurangi subduction zone, New Zealand, *Science*, *352*(6286), 701–704.

Walter, J. I., S. Y. Schwartz, M. Protti, and V. Gonzalez (2013), The synchronous occurrence of shallow tremor and very low frequency earthquakes offshore of the Nicoya Peninsula, Costa Rica, *Geophys. Res. Lett.*, *40*, 1517–1522, doi:10.1002/grl.50213.

Wang, K., and S. L. Bilek (2011), Do subducting seamounts generate or stop large earthquakes?, *Geology*, *39*(9), 819–822.

Wdowinski, S., Y. Bock, J. Zhang, P. Fang, and J. Genrich (1997), Southern California permanent GPS geodetic array: Spatial filtering of daily positions for estimating coseismic and postseismic displacements induced by the 1992 Landers earthquake, *J. Geophys. Res.*, *102*(B8), 18,057–18,070, doi:10.1029/97JB01378.

Wech, A. G., and K. C. Creager (2008), Automated detection and location of Cascadia tremor, *Geophys. Res. Lett.*, *35*, L20302, doi:10.1029/2008GL035458.

Worzewski, T., M. Jegen, H. Kopp, H. Brasse, and W. T. Castillo (2011), Magnetotelluric image of the fluid cycle in the Costa Rican subduction zone, *Nat. Geosci.*, *4*(2), 108–111.

Yue, H., T. Lay, S. Y. Schwartz, L. Rivera, M. Protti, T. H. Dixon, S. Owen, and A. V. Newman (2013), The 5 September 2012 Nicoya, Costa Rica M_w 7.6 earthquake rupture process from joint inversion of high-rate GPS, strong-motion, and teleseismic *P* wave data and its relationship to adjacent plate boundary interface properties, *J. Geophys. Res. Solid Earth*, *118*, 5453–5466, doi:10.1002/jgrb.50379.

Zumberge, J. F., M. B. Heflin, D. C. Jefferson, M. M. Watkins, and F. H. Webb (1997), Precise point positioning for the efficient and robust analysis of GPS data from large networks, *J. Geophys. Res.*, *102*(B3), 5005–5017, doi:10.1029/96JB03860.